CALPHAD: Computer Coupling of Phase Diagrams and Thermochemistry 43 (2013) 1–6

Contents lists available at ScienceDirect

CALPHAD: Computer Coupling of Phase Diagrams and Thermochemistry

journal homepage: www.elsevier.com/locate/calphad

Crystallographic characterization of Cu–In alloys in the 30–37 at% In region

L. Baqué [a,1], D. Torrado [b], D.G. Lamas [a,b], S.F. Aricó [c], A.F. Craievich [d], S. Sommadossi [a,b,*]

[a] CONICET, CCT-Comahue, Buenos Aires 1400, 8300 Neuquén, Argentina
[b] Fac. de Ingeniería-UNComahue, Buenos Aires 1400, 8300 Neuquén, Argentina
[c] Depto. de Materiales, CAC-CNEA, Av. Gral. Paz 1499 B1650KNA San Martín, Argentina
[d] Institute of Physics—University of São Paulo, Rua do Matao, Travessa R, 187, CEP05508-900 São Paulo, Brazil

ARTICLE INFO

Article history:
Received 20 April 2013
Received in revised form
31 July 2013
Accepted 13 August 2013
Available online 30 August 2013

Keywords:
Cu–In alloys
Powder diffraction
Phase equilibrium
Crystallography
Superlattices

ABSTRACT

The Cu–In–Sn system is one of the Pb-free options to replace conventional Pb–Sn alloys in electronic industry. However, controversies still exist regarding some regions of the equilibrium phase diagram of the Cu–In–Sn ternary and also of the Cu–In and Cu–Sn binary systems. One of the most controversial fields of the Cu–In binary phase diagram lies between ~33 and 38 at% In and temperatures ranging from 100 up to 500 °C. In this work, binary Cu–In alloys, with 30–37 at% In nominal compositions and annealed at two different temperatures (i.e. 300 °C and 500 °C) for a long period (i.e. 7 months) were characterized by scanning electron microscopy (SEM), wavelength dispersive spectroscopy (WDS) and X-ray diffraction (XRD). Three phases exist over the 33–38 at% In composition range, namely the phase A at high temperatures and the B and C phases at low temperatures. These three phases can be described as superstructures of the hexagonal phase *h* (Cu_2In) and differ, although slightly, from those previously reported in the literature. In addition, it has been demonstrated that even conventional XRD allows to unequivocally distinguishing between these phases despite their similar crystal structure.

1. Introduction

n last decades, an increasing number of new regulations were issued all over the world with the aim of preserving the environment. In particular, one of the current goals of electronic industry is to decrease or even eliminate the use of Pb in solders [1,2]. Sn–In alloys are attractive as Pb-free solders since they exhibit low melting temperatures [1–3]. In addition, these alloys are suitable to joint Cu substrates (which are usually employed in electronic industry) by transient liquid phase bonding (TLPB) [4,5]. This method involves the melting of the Sn–In interlayer and the formation of solid phases by interdiffusion or reaction diffusion. The resultant intermetallic phases have a melting and maximum operation temperature that can be several hundred Celsius degrees higher than the processing temperature.

It has been previously reported that η-$Cu_6(Sn,In)_5$, ζ-$Cu_{10}(Sn,In)_3$, η-$Cu_2(In,Sn)$, δ-$Cu_7(In,Sn)_3$ phases are formed at the interconnec tion zone in the Cu/In–48Sn/Cu system [6,7]. These intermetallic compounds correspond to binary phases capable of including small quantities of a third element (i.e. In either Sn) in their crystal structure. Nevertheless, several discrepancies still remain concerning not only the Cu–In–Sn ternary phase diagram but also the Cu–In, Cu–Sn and In–Sn binary diagrams [2]. In particular, η-Cu_2In phase belongs to one of the most controversial fields of the Cu–In binary phase diagram which lies between ~33 and 38 at% In and temperatures ranging from 100 up to 500 °C (see Fig. 1a). Therefore, the further study of this region is needed for the practical application of Sn–In soldering alloys in the electronic industry.

Fig. 1a shows the Cu–In phase diagram proposed by Subramanian and Laughlin [8]. The η field in this diagram is based in several previous researches, but mainly in the work by Jain et al. [9]. These authors reported five different phases named as *h*, A and A′ for high temperature, and B and C for low temperature in the 33–38 at% In range. The crystal structure of the phase *h* is full known [10] and can be described with a hexagonal cell. Phases A (PDF 00-026-0523 card) and A′ (PDF 00-026-0522 card) have been assigned orthorhombic cells with a volume ten times and sixteen times larger than the parent hexagonal cell, respectively. No crystallographic cells for B and C phases were proposed in that work.

The results of further investigations carried by Bolcavage and others led to the phase diagram shown in Fig. 1b [11,12]. This diagram indicates that only two phases occur in the 33–38 at% In composition/temperature range, namely η and η′, at low and high temperatures, respectively. The η+η′ field seems to be widely

* Corresponding author at: Fac. de Ingeniería, UNComahue, Buenos Aires 1400, 8300 Neuquén, Argentina. Tel.: +54 299 4490300 int. 653.
E-mail addresses: ssommadossi@gmail.com, silvana.sommadossi@fain.uncoma.edu.ar (S. Sommadossi).
[1] Present address: Department of Energy Conversion and Storage, Technical University of Denmark, Frederiksborgvej 399, DK-4000 Roskilde, Denmark.

0364-5916/$ - see front matter © 2013 Published by Elsevier Ltd.
http://dx.doi.org/10.1016/j.calphad.2013.08.005

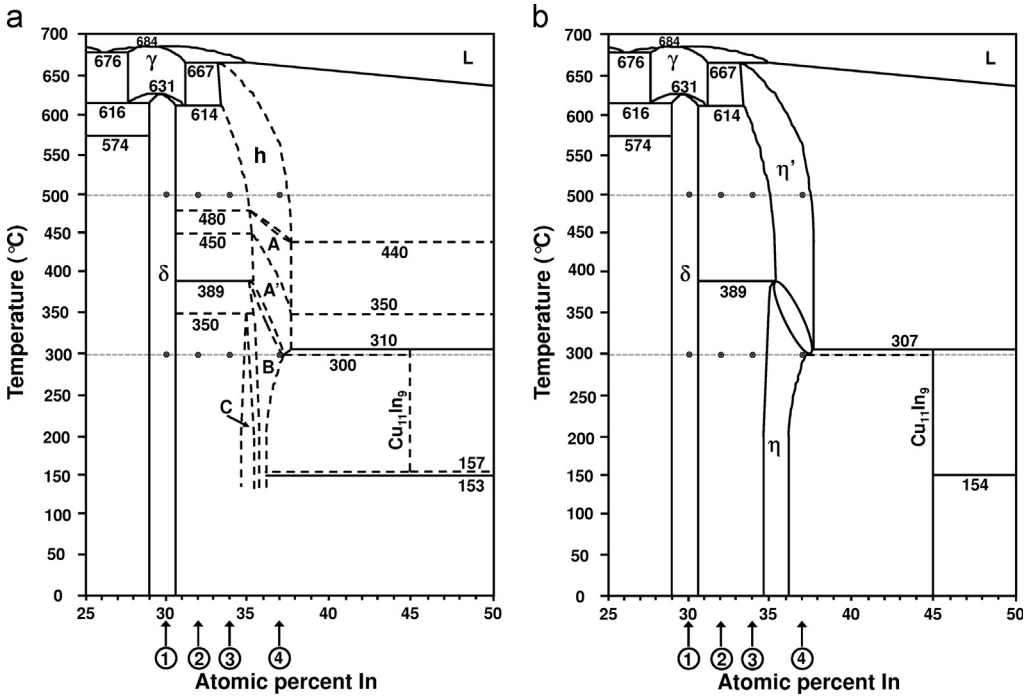

Fig. 1. Cu–In phase diagram according to (a) P. R. Subramanian, D.E. Laughlin [8] and (b) Bolcavage et al. [11]. Nominal composition and annealing temperature of samples studied in this work are also indicated.

accepted as it was incorporated in the subsequent updated Cu–In phase diagrams reported by Okamoto [13,14]. η′ phase presents the same crystal structure of phase h [8,10]. Some X-ray diffraction (XRD) data for phases η and η′ were reported by Bolcavage [11] although they seemed inconsistent.

On the other hand, Elding-Pontén et al. [15] proposed that the η+η′ field is composed of three distinct phases, namely A at high temperatures and B and C at low temperatures. These author described phase A and B as a 10a × 10b × 1c supercell of the hexagonal cell related to phase h whereas phase C was described with an orthorhombic cell. These phases would transform one to another with the continuous rotation of the sub-motif in the electron diffraction pattern. The phase A′ reported by Jain et al. [9] have not been detected by Elding-Pontén et al. [15] and it would be incorporated in the A phase.

As a result, electron and X-Ray diffraction data reported in literature for different phases within the 33–38 at% In region tend to be puzzling. In general, all these phases can be described as NiAs–Ni_2In-type superstructures [8,15,16]. The principal reflections of the related diffraction patterns can be indexed with an hexagonal cell, whereas the remaining reflections present low intensity and are related to domain twining [15,16]. Accordingly, the accurate identification of crystal structure is very difficult. Moreover, in most of the works found in literature, the peak intensity of powder diffraction patterns is visually estimated and hence data comparison can be quite cumbersome.

Further research combining several characterization techniques is required in order to elucidate the controversies mentioned above. This work aims at characterizing binary Cu–In alloys, with 30–37 at% In nominal compositions and annealed at two different temperatures (i.e. 300 °C and 500 °C) for 7 months. These annealing times, which are far longer that those usually reported in the literature, were specially chosen in order to ensure a good phase homogenization. Composition determination and phase identification were performed by wavelength dispersive spectroscopy (WDS) and scanning electron microscopy. In addition, the crystallographic features of these alloys were investigated by X-ray powder diffraction (XRD).

Table 1
Nominal composition, annealing temperature and phase contents in the different samples studied in this work.

Sample name	Nominal composition		Annealing temperature (°C)	Present phases
	at% In[a]	at% Cu		
S1-500	30	70	500	Phase δ (Cu_7In_3) [17]
S2-500	32	68	500	Phase δ (Cu_7In_3) [17]+ Phase A [this work, 15]
S3-500	34	66	500	Phase δ (Cu_7In_3) [17]+ Phase A [this work, 15]
S4-500	37	63	500	Phase A [this work, 15]
S1-300	30	70	300	Phase δ (Cu_7In_3) [17]
S2-300	32	68	300	Phase δ (Cu_7In_3) [17]+ Phase C [15]
S3-300	34	66	300	Phase δ (Cu_7In_3) [17]+ Phase C [15]
S4-300	37	63	300	Phase B [this work, 15]

[a] The experimental error in the sample composition (i.e. the difference between the nominal and the actual composition of the sample) is up to ± 1 at% In.

2. Experimental

Eight samples with nominal composition within 30–37 at% In range were prepared. 99.999% Cu and 99.999% In ingots were melted together under Ar atmosphere and then the melt was cooled down to room temperature. Four samples were subsequently annealed during 7 months at 300 °C under Ar atmosphere and then quenched down to room temperature. The same procedure was applied to the remaining samples but in this case at 500 °C. Nominal composition and annealing temperature of all studied samples are indicated in Fig. 1 and listed in Table 1.

The morphology of the samples was analyzed by using a Philips 515 SEM. Images were acquired with backscattered electrons in order to maximize atomic number contrast.

Lineal composition profiles with 1–4 μm steps were determined by using the WDS technique employing a Cameca SX50

Table 2
Literature crystal structure data used for identifying the phases present in the samples investigated in the present work.

Name	Stoichiometry	Space group symbol	Pearson symbol	Lattice parameters	PDF/ICSD card	Ref.
η' (or h)	$Cu_{0.66}In_{0.33}$	$P6_3/mmc$	hP6	a=4.294 Å c=5.233 Å	PDF 03-065-0704	[9,10]
A	$Cu_{0.64}In_{0.36}$	Orthorhombic system	oP50	a=21.375 Å b=7.405 Å c=5.218 Å	PDF 00-026-0523	[9]
A′	$Cu_{0.64}In_{0.36}$	Orthorhombic system	oP75	a=34.194 Å b=7.395 Å c=5.262 Å	PDF 00-026-0522	[9]
A	33–40 at% In	$P6_3/mmc$	hP600	a=42.747 Å c=5.262 Å	–	[15]
B	34–37 at% In	$P6_3/mmc$	hP600	a=42.747 Å c=5.262 Å	–	[15]
C	$Cu_{0.66}In_{0.34}$	Orthorhombic system	No reported	a=38.391 Å b=7.388 Å c=20.972 Å	–	[15]
Cu_7In_3	$Cu_{0.7}In_{0.3}$	P-1	aP40	a=6.733 Å b=9.134 Å c=10.074 Å α=73.20° β=82.77° γ=89.76°	PDF 01-073-8028	[17]

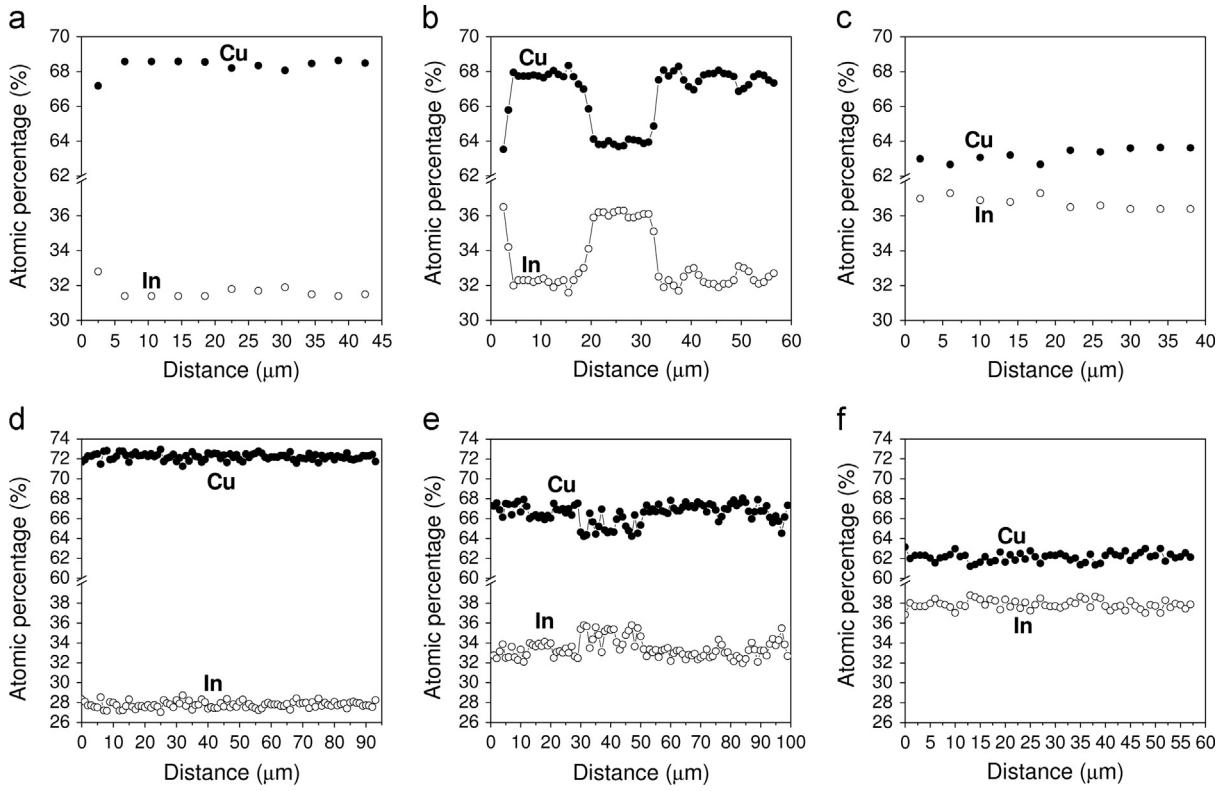

Fig. 2. Composition profile of selected samples determined by WDS with a beam diameter of 1 μm. (a) S1-500, (b) S3-500, (c) S4-500, (d) S1-300, (e) S2-300 and (f) S4-300.

electron microprobe under an accelerating potential of 20 kV. The equipment was recalibrated before each analysis session using pure 99.999 wt% Cu and 99.999 wt% In standards.

Fine powders for XRD measurements were obtained by milling the alloys in an agate mortar and then sieving them through a 20 μm mesh. XRD experiments were performed using a Philips PW1700 diffractometer with Cu K_α radiation and a graphite monochromator. Powder diffraction patterns were recorded over the $10^\circ \leq 2\theta \leq 90^\circ$ range with 0.02° step and 10 s/step counting time. Phase identification was performed by analyzing the positions and intensities of all the peaks observed in each diffractogram and comparing them with those previously reported in the literature. The crystal structure data of the relevant phases reported in literature are summarized in Table 2.

3. Results and discussion

3.1. Characterization of composition and morphology

Composition profiles of all samples studied in this work were determined by WDS, whereas their morphology was observed by SEM. Samples with nominal composition of 30 and 37 at.% In (i.e. S1-500, S1-300, S4-500 and S4-300) consist of only one single phase while specimens with 32 and 34 at% In nominal composition (i.e. S2-500, S2-300, S3-500 and S3-300) present two phases. These observations are in agreement with both phase diagrams shown in Fig. 1.

Composition of sample S1-500 matches that of the δ phase (Cu_7In_3), as can be observed in Fig. 2a. Sample S4-500 has a composition of 37 at% In and 63 at% Cu (see Fig. 2c). This composition can correspond to h phase (see Fig. 1a), phase η' (see Fig. 1b) or phase A [15]. Fig. 2b shows that sample S3-500 is composed of two phases (see also Fig. 3a): one with the composition of sample S1-500 (phase δ) and another with composition similar to that of sample S4-500. Similar results were obtained for sample S2-500, although with higher proportion of phase δ and lower proportion of the other one (not shown).

The composition of the S1-300 sample corresponds to phase δ (see Fig. 2d), as indicated in both phase diagrams displayed in Fig. 1. S2-300 and S3-300 samples contain both the same two phases but in different proportions. The composition profile and the microstructure of the S2-300 sample are shown in Figs. 2e and 3b, respectively. The dark zone in Fig. 3b has a composition of ~33 at% In/67 at% Cu, while the composition of the bright zone is ~35 at% In/65 at% Cu. It is worth noticing the particular features of

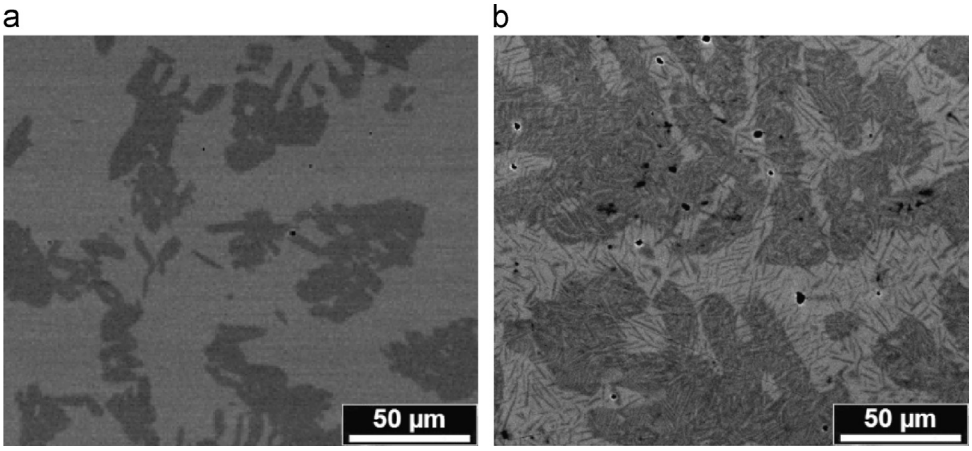

Fig. 3. SEM images acquired with backscattering electrons from samples (a) S3-500 and (b) S2-300.

the microstructure of these phase mixture, which consists of needles of one phase growing inside the matrix of the other phase. The changes in the composition occur within a distance that is shorter than the beam diameter (~1 μm) used for WDS and hence the composition of each point corresponds to the mixture of two phases. This causes an overestimation of In content in the dark zone and an underestimation in the bright zone. This kind of microstructure was also observed by Jain et al. [9] in a $Cu_{66}In_{34}$ sample annealed at 560 °C for two days and then at 370 °C for seven days, although these authors assign this behavior to the formation of phase B. Fig. 2f shows that sample S4-300 has a composition ~38 at% In/62 at% Cu, which correspond to a biphasic region. However, the error in the WDS measurements was estimated to be~0.4 at% In and hence, the actual composition of the S4-300 sample is~37.6 at% In/62.4 at% Cu. According to the lever rule and the phase diagrams of Fig. 1, this composition corresponds to a mixture of 4 wt% of phase $Cu_{11}In_9$ and 96 wt% of phase B either phase η.

3.2. Crystallographic characterization

Powder XRD experiments were performed in order to identify precisely which phases are present in $Cu_{100-x}In_x$ samples with $x > 30$ (see Table 1). Fig. 4a shows XRD patterns corresponding to samples annealed at 500 °C. The XRD pattern corresponding to sample S1-500 matches the pattern expected for δ phase (Cu_7In_3- PDF 01-073-8028 card). This result is in agreement with the WDS data reported in the previous section and with both phase diagrams shown in Fig. 1. The XRD pattern corresponding to sample S4-500 can be related to the phase A reported by Elding-Pontén et al. [15] XRD patterns corresponding to S2-500 and S3-500 samples exhibit several peaks related to both δ and A phases. The intensity of peaks related to phase δ diminishes with In content while the intensity of those related to phase A increases (see enlarged region displayed in Fig. 4b). This implies that the proportion of phase δ decreases while the proportion of phase A increases for increasing In content.

XRD patterns corresponding to samples annealed at 300 °C are displayed in Fig. 5a. All peaks of the pattern referring to sample S1-300 can be assigned to phase δ (Cu_7In_3- PDF 01-073-8028 card). The features of the XRD patterns corresponding to samples S2-300 and S3-300 indicate that these samples are composed of both δ and C phases. The intensity of peaks associated to phase C is stronger in the XRD pattern corresponding to the S3-300 sample, this feature indicating that the proportion of phase C in this sample is higher than in S2-300 (see Fig. 5b). All peaks observed in the XRD pattern of sample S4-300 can be associated to the phase B previously reported by Elding-Pontén et al. [15]. According

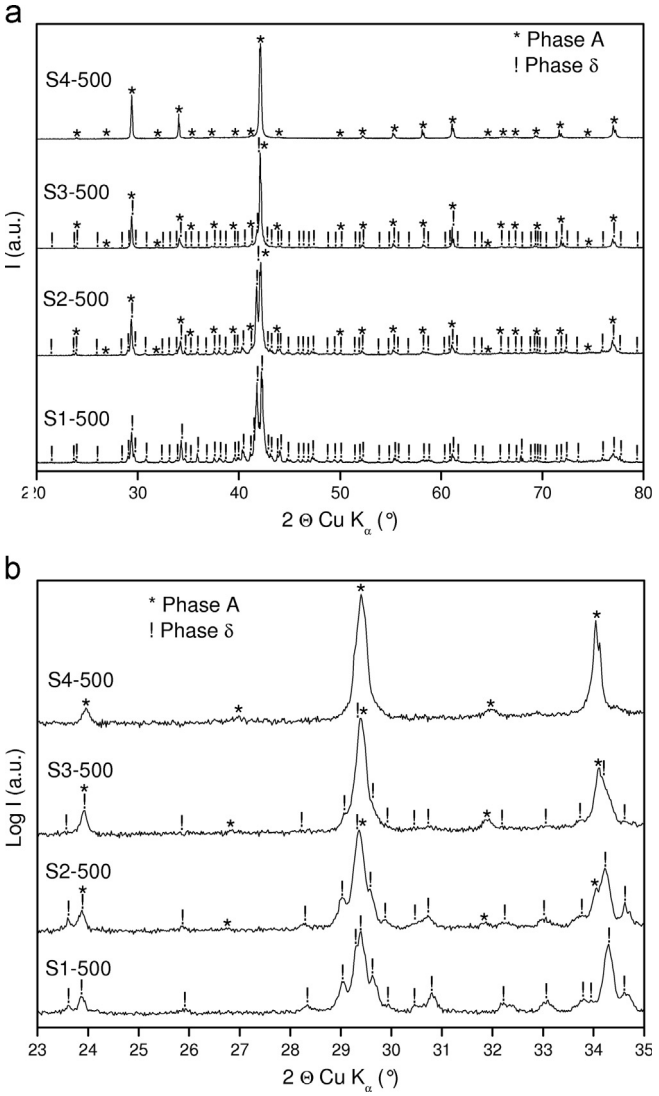

Fig. 4. X-Ray diffraction patterns corresponding to Cu–In samples annealed at 500 °C. (a) Full XRD patterns. (b) Reduced 2θ range over which the effects on XRD patterns produced by the variation in phase content associated to different composition can clearly be noticed. Symbols indicate the position of reflections corresponding to each phase.

to the composition of sample S4-300 determined by WDS (see Section 3.1) and the phase diagrams of Fig. 1, this sample would contain~4 wt% of phase $Cu_{11}In_9$. X-ray diffraction pattern

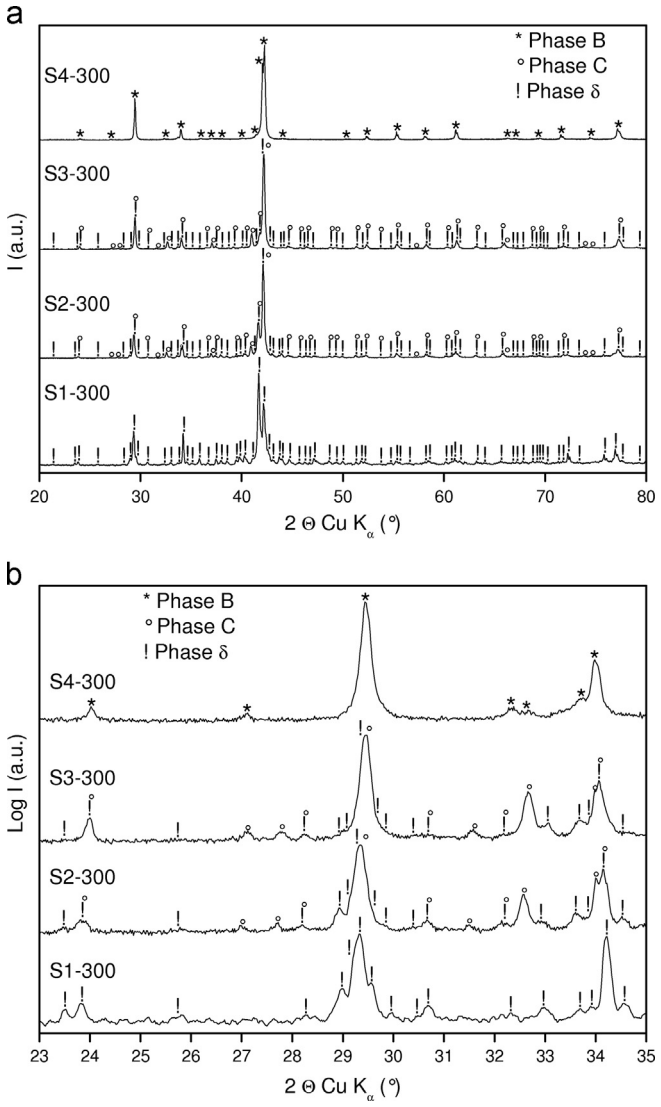

Fig. 5. X-Ray diffraction patterns corresponding to samples annealed at 300 °C. (a) Full X-ray patterns and (b) reduced 2θ range in which the variation in phase content for different compositions can clearly be noticed. Symbols indicate the position of Bragg peaks corresponding to each phase.

Table 3
Position, interplanar distance, relative intensity and *hkl* indexes of reflections corresponding to phase A and phase B.

Phase A						Phase B					
2θ (°)	d_{phkl} (Å)	Relative intensity (%)	*h*	*k*	*l*	2θ (°)	d_{hkl} (Å)	Relative intensity (%)	*h*	*k*	*l*
23.973[a]	3.712	1.49	10	0	0	24.033[a]	3.703	1.34	10	0	0
26.850[b]	3.321	0.25									
						27.118	3.288	0.76	7	6	0
29.403[a]	3.038	48.08	10	0	1	29.442[a]	3.034	43.35	10	0	1
31.946[b]	2.802	0.98	10	5	0						
						32.343[b]	2.768	1.12	8	5	1
						32.716[b]	2.737	0.61	13	1	0
						33.685[b]	2.661	2.3	12	0	1
34.038[a]	2.632	26.84	0	0	2	33.972[a]	2.639	10.71	0	0	2
35.396	2.534	1.63	4	0	2						
						36.023[b]	2.493	1.25	9	6	1
						36.816[b]	2.441	1.42	11	4	1
						37.097[b]	2.424	1.4	4	3	2
37.311[b]	2.408	1.57	13	4	0	37.464	2.401	0.96	13	4	0
						38.056[b]	2.365	1.09	10	6	1
39.576	2.275	1.03	13	3	1						
						40.028[b]	2.253	1.42	8	1	2
41.206	2.189	2.87	13	4	1						
						41.414	2.180	5.03	9	1	2
42.041[a]	2.147	90.09	10	0	2	42.058[a]	2.147	79	10	0	2
42.157[a]	2.142	100	10	10	0	42.254[a]	2.137	100	10	10	0
43.926	2.060	0.81	7	6	2	44.033	2.055	1.06	7	6	2
50.005[b]	1.823	0.35	12	10	1						
						50.241	1.815	0.48	13	9	1
52.216[a]	1.750	2.85	20	0	1	52.343[a]	1.746	3.66	20	0	1
55.235[a]	1.662	5.69	10	10	2	55.313[a]	1.660	8.35	10	10	2
58.123[a]	1.586	9.62	10	0	3	58.101[a]	1.586	3.79	10	0	3
61.064[a]	1.516	15.07	20	0	2	61.160[a]	1.514	10.38	20	0	2
64.532	1.443	0.42	23	3	1						
66.025	1.414	0.88	23	4	1						
						66.278	1.409	1.31	14	3	3
67.257	1.391	0.77	24	3	1	67.091	1.394	1.01	24	3	1
69.298[a]	1.355	2.19	20	10	1	69.451[a]	1.352	1.62	20	10	1
71.664[a]	1.316	8.68	0	0	4	71.551[a]	1.318	4.96	0	0	4
74.342[a]	1.275	0.98	20	0	3	74.432[a]	1.274	2.19	20	0	3
77.001[a]	1.237	13.53	20	10	2	77.144[a]	1.235	10.98	20	10	2
						82.906	1.164	0.31	27	7	1
86.811[a]	1.121	13.37	10	10	4	86.796[a]	1.121	7.58	10	10	4

[a] Indicate the reflections that also match *h* phase (Cu_2In, PDF 03-065-0704 card).
[b] Indicate the reflections that were not reported by Elding-Pontén et al. [15].

simulations performed with FullProf Suite [18,19] indicate that in this case the distinct peaks of phase $Cu_{11}In_9$ should have very low intensity and do not overlap the low intensity peaks of phase B. Therefore, although the presence of phase $Cu_{11}In_9$ cannot be absolutely discarded, the crystallographic analysis regarding phase B will be unaffected by this issue. It is worth noticing that the composition range of the phases B and C is still not clearly defined in the literature. Elding-Pontén et al. [15] observed the presence of phase B in samples with 34 and 37 at% In composition and the presence of phase C only in samples with 34 at% In composition. Previously, Jain et al. [8,9] reported a narrow composition range for both phases: 35.6–37.3 at% In for phase B and 34.1–35.2 at% In for phase C. In order to investigate the composition range of each individual phase as well as the coexistence range, further X-ray and also TEM measurements in samples with lower composition differences (i.e. 0.5 at% In) are required.

Angular position, interplanar distance, relative intensity and *hkl* indexes of X-ray Bragg reflections corresponding to A and B phases are listed in Table 3. The main reflections of both phases (indicated as (a) in Table 3) match those of phase *h* (Cu_2In, PDF 03-065-0704 card). This phase can be represented by a hexagonal cell belonging to $P6_3/mmc$ space group. Cell parameters determined from the angular positions of Bragg peaks are $a=4.286$ Å and $c=5.263$ Å ($c/a=1.233$) for phase A and $a=4.276$ Å and $c=5.278$ Å ($c/a=1.234$) for phase B, these values being in agreement with those expected for 37–38 at% In composition [10]. The remaining low intensity reflections are related to an effect of domain twining [15,16], yielding a superstructure of the Cu_2In phase. Superstructure reflections of both A and B phases were indexed with a $10a \times 10b \times 1c$ supercell, as it was previously proposed by Elding-Pontén et al. [15] based on XRD and electron diffraction data. It is worth pointing out that not all reflections reported by Elding-Pontén et al. [15] for A and B phases were observed in our XRD patterns. Moreover, a few additional low intensity reflections (indicated as (b) in Table 3) detected in our XRD patterns were not reported by these authors (see Table 3). Samples studied by Elding-Pontén et al. [15] were annealed over three weeks at temperatures within the 400–500 °C range for phase A and within the 250–350 °C range for phase B, while the samples studied in the present work were annealed during seven months at 500 °C and 300 °C, respectively. In order to establish the influence of sample preparation conditions (i.e. temperature, annealing time, cooling

treatment, etc.) on the crystal structures further investigations are needed.

Only one low intensity Bragg peak corresponding to phase A (i.e. 2 θ=26.85°, relative intensity=0.25) could not be indexed by considering the 10a × 10b × 1c supercell. Several attempts were made by applying *Supercell* program within FullProf Suite [18,19] to find a suitable supercell by taking into account all reflections observed for phase A, although with no success. Additional electron diffraction experiments are planned in order to further investigate this issue. Alternatively, the XRD pattern corresponding to phase A was indexed with a monoclinic cell using DICVOL06 program [20]. Cell parameters were refined with the Le Bail method [21] yielding a=6.018, b=15.725, c=3.724 and β=95.24°. The resultant reliability factors were quite good, indicating that the refined cell parameters are correct. However, more than one hundred atoms are needed to describe the parent structure (i.e. Cu_2In – ICSD 657611 card) using the monoclinic cell, and therefore the identification of structure distortions is extremely difficult.

The results reported here for the 34–37 at% In composition range are in agreement with those previously reported by Elding-Pontén et al. [15]. At low temperature (i.e. 300 °C), our results are also in accordance with the phase diagram proposed by Jain et al. [9] (Fig. 1a) while they differ from what is expected from the phase diagram shown Fig. 1b (Bolcavage et al. [11]) that indicates the presence of only one phase (η). According to the phase diagrams displayed in Fig. 1, sample S4-500 is expected to contain phases h or η′ (both with identical crystal structure). Instead, we have established that this sample only contains phase A (Table 3), which is a superstructure of phase h (Cu_2In, PDF 03-065-0704 card) and differs from phases A (PDF 00-026-0523 card) and A′ (PDF 00-026-0522 card) previously reported by Jain et al. [9].

Beside the difficulty encountered to fully describe the crystal structure of phases A and B, it is worth noticing that XRD data listed in Table 3 are useful for the identification of their phase contents. Although A, B and C phases exhibit similar crystal structure, the superstructure reflections that characterize them are quite intense and can be easily detected even by using a conventional powder XRD setup (see Figs. 4b and 5b and Table 3). According to the data from Elding-Pontén et al. [15] and to our own data presented in this work, the phases A, B and C can be distinguished by their different diffraction patterns. This is also possible because of the different symmetry of each phase. In the case in which two samples correspond to the same phase but have different compositions, the diffractograms would differ slightly in the angular positions and intensities of the Bragg peaks (see for example reference [10]). Consequently, the results derived from the XRD patterns allowed us a clear identification of each phase, while, by only applying SEM and/or WDS, the same cannot be achieved.

4. Conclusions

The phases present in binary Cu–In alloys, with 30–37 at% In nominal compositions and annealed for 7 months at two different temperatures (i.e. 300 °C and 500 °C) were characterized by scanning electron microscopy (SEM), wavelength dispersive spectroscopy (WDS) and X-ray diffraction (XRD).

Our results indicate the presence of three phases over the Cu 33–38 at% In composition range, namely the A phase at high temperatures (i.e. 500 °C) and the B and C phases at low temperatures (i.e. 300 °C). There are in good agreement with those previously reported by Elding-Pontén et al. [15]. Phase A is a superstructure of phases h or η′ (both with identical crystal structure) [8–12] and differs from phases A (PDF 00-026-0523 card) and A′ (PDF 00-026-0522 card) previously reported by Jain et al. [9]. At low temperature, the existence of phases B and C is in accordance with the phase diagram proposed by Jain et al. [9] while they differ from the only one phase (η) expected from the phase diagram proposed by Bolcavage et al. [11].

The lattice parameters of phases A and B were determined. All powder XRD patterns corresponding to both identified phases were indexed under the assumption of a 10a × 10b × 1c supercell as proposed by Elding-Pontén et al. [15]. Nevertheless, XRD patterns collected in our work for phases A and B do not present all reflections reported by those authors and still present a few additional low intensity reflections.

The data obtained in this work are expected to be useful for further phase identification of the studied alloys. On the other hand, we have shown that XRD even using a conventional diffraction setup can unequivocally distinguish between A, B and C phases, the same not being accomplished by only using SEM and/or WDS techniques.

Acknowledgments

L. Mogni, A. Serquis and A. Caneiro are gratefully acknowledged for XRD experiments at CAB-CNEA. The authors thank G. Aurelio for manuscript revision. This work was funded by FONCyT Projects PICT 2006-1947, PICT 2010-2176, Comahue National University and CONICET.

References

[1] A.T. Dinsdale, A. Watson, A. Kroupa, J. Vrestal, A. Zemanova, J. Vízdal (Eds.), COST Action 531 – Atlas of Phase Diagrams for Lead-Free Soldering, vol. 1–2, COST Office, Brussels, 2008.
[2] S.-W. Chen, C.-H. Wang, S.-K. Lin, C.-N. Chiu, Phase diagrams of Pb-free solders and their related materials systems, J. Mater. Sci.: Mater. Electron. 18 (2007) 19–37.
[3] G. Zeng, S. Xue, L. Zhang, L. Gao, Recent advances on Sn–Cu solders with alloying elements: review, J. Mater. Sci.: Mater. Electron. 22 (2011) 565–578.
[4] W.F. Gale, D.A. Butts, Transient liquid phase bonding, Sci. Technol. Weld. Joining 9 (2004) 283–300.
[5] G.O. Cook III, C.D. Sorensen, Overview of transient liquid phase and partial transient liquid phase bonding, J. Mater. Sci. 46 (2011) 5305–5323.
[6] S. Sommadossi, W. Gust, E.J. Mittemeijer, Characterization of the reaction process in diffusion-soldered Cu/In–48 at% Sn/Cu joints, Mater. Chem. Phys. 77 (2002) 924–929.
[7] S. Sommadossi, A.F. Guillermet, Interface reaction systematics in the Cu/In–48Sn/Cu system bonded by diffusion soldering, Intermetallics 15 (2007) 912–917.
[8] P.R. Subramanian, D.E. Laughlin, The Cu–In system, Bull. Alloy Phase Diagrams (1989)554–610 (references therein).
[9] K.C. Jain, M. Ellner, K. Schubert, Über die pahsen in der nähe der zusammensetzung Cu64In36, Z. Metallkde. 63 (1972) 456–461.
[10] G.C. Che, M. Ellner, Powder crystal data for the high-temperature phases Cu4In, Cu9In4 (h) and Cu2In (h), Powder Diffr. 7 (1992) 107–108.
[11] A. Bolcavage, S.W. Chen, C.R. Kao, Y.A. Chang, A.D. Romig Jr., Phase equilibria of the Cu–In system I: experimental investigation, J. Phase Equilibria 14 (1993) 14–21.
[12] Z. Bahari, E. Dichi, B. Legendre, J. Dugué, The equilibrium phase diagram of the copper–indium system: a new investigation, Thermochim. Acta 401 (2003) 131–138.
[13] H. Okamoto, Comment on Cu–In, J. Phase Equilibria 15 (1994) 226–227.
[14] H. Okamoto, J. Cu-In, Phase Equilibria and Diffusion 26 (2005) 645.
[15] M. Elding-Pontén, L. Stenberg, S. Lidin, The η-phase field of the Cu–In system, J. Alloys Compd. 261 (1997) 162–171.
[16] S. Lidin, A.-K. Larsson, A survey of superstructures in intermetallic NiAs–Ni2In-type phases, J. Solid State Chem. 118 (1995) 313–322.
[17] S. Lidin, L. Stenberg, M. Elding-Pontén, The B8 type structure of Cu7In3, J. Alloys Compd. 255 (1997) 221–226.
[18] J. Rodríguez-Carvajal, Recent advances in magnetic structure determination by neutron powder diffraction, Phys. B: Condens. Matter 192 (1993) 55–69.
[19] J. Rodríguez-Carvajal, Recent developments of the program FULLPROF, Comission on Powder Diffr. (IUCr) Newsl. 26 (2001) 12–19.
[20] A. Boultif, D. Louër, Powder pattern indexing with the dichotomy method, J. Appl. Crystallogr. 37 (2004) 724–731.
[21] A. Le Bail, H. Duroy, J.L. Fourquet, Ab-initio structure of LiSbWO6 by X-ray powder diffraction, Mat. Res. Bull. 23 (1998) 447–452.